In vitro selection of the Naegleria GIR1 ribozyme identifies three base changes that dramatically improve activity

E. Jabri and T. R. Cech

RNA 1998 4: 1481-1492

RNA (1998), *4*:1481–1492. Cambridge University Press. Printed in the USA.

In vitro selection of the *Naegleria* GIR1 ribozyme identifies three base changes that dramatically improve activity

EVELYN JABRI and THOMAS R. CECH

Department of Chemistry and Biochemistry, Howard Hughes Medical Institute, University of Colorado, Boulder, Colorado 80309-0215, USA

ABSTRACT

NanGIR1 is a member of a new class of group I ribozymes whose putative biological function is site-specific hydrolysis at an internal processing site (IPS). We have previously shown that NanGIR1 requires 1 M KCl for maximal activity, which is nevertheless slow (0.03 min^{-1}). We used in vitro selection and an RNA pool with approximately nine mutations per molecule to select for faster hydrolysis at the IPS in 100 mM KCl. After eight rounds of selection, GIR1 variants were isolated that catalyzed hydrolysis at 300-fold greater rates than NanGIR1 RNA. Although not required by the selection, many of the resultant RNAs had increased thermal stability relative to the parent RNA, and had a more compact structure as evidenced by their faster migration in native gels. Although a wide spectrum of mutations was found in generation 8 clones, only two mutations, U149C and U153C, were common to greater than 95% of the molecules. These and one other mutation, G32A, are sufficient to increase activity 50-fold. All three mutations lie within or proximal to the P15 pseudoknot, a structural signature of GIR1 RNAs that was previously shown to be important for catalytic activity. Overall, our findings show that variants of the *Naegleria* GIR1 ribozyme with dramatically improved activity lie very close to the natural GIR1 in sequence space. Furthermore, the selection for higher activity appeared to select for increased structural stability.

Keywords: crystallography; hydrolysis; in vitro selection; pseudoknot; ribozymes; RNA folding; RNA catalysis

INTRODUCTION

In vitro selection is a powerful method to identify the diverse catalytic functions of RNA (Bartel & Szostak, 1993; Szostak & Ellington, 1993; Tsang & Joyce, 1994; Tarasow et al., 1997; Zhang & Cech, 1997). It has also been used to change the activity of a particular RNA under specific conditions, such as alteration of the divalent metal ion requirements of various ribozymes including group I introns (Lehman & Joyce, 1993a,b) and RNase P (Frank & Pace, 1997). In addition, in vitro selection is ideal for generating an artificial phylogeny from which key nucleotides for specific catalytic functions can be identified.

Some group I introns from *Didymium* and *Naegleria* contain an internal catalytic element called GIR1 (group I ribozyme) (Decatur et al., 1995; Einvik et al., 1997). These sequences are themselves stripped down group I introns whose putative biological function is site-specific hydrolysis at an internal processing site (IPS) to form the 5′ end of the downstream mRNA (Fig. 1). We have shown that NanGIR1 (the *Naegleria andersoni* ribozyme) cleaves itself two orders of magnitude faster than the *Tetrahymena* 3′ splice site hydrolysis reaction, but is still three orders of magnitude slower than RNase P (Jabri et al., 1997). In addition, NanGIR1 requires >500 mM K^+ for catalysis, which we speculate substitutes for a protein cofactor that associates with this RNA in vivo.

Structurally, NanGIR1 has many of the elements of a group I intron, but it lacks the P1 pairing element that includes the 5′ splice site, as well as other nucleotides important for self splicing. Also in contrast to group I introns, NanGIR1 has a novel P15 pseudoknot, which was shown by site-directed mutagenesis to be critical for catalytic activity (Jabri et al., 1997; Einvik et al., 1998). Furthermore, chemical modification studies in conjunction with site-directed mutagenesis have suggested that this structural element is dynamic. Se-

Reprint requests to: Dr. Thomas R. Cech, Department of Chemistry and Biochemistry, Campus Box 215, University of Colorado, Boulder, Colorado 80309-0215, USA; e-mail for Thomas R. Cech: thomas.cech@colorado.edu; e-mail for Evelyn Jabri: jabri@petunia.colorado.edu.

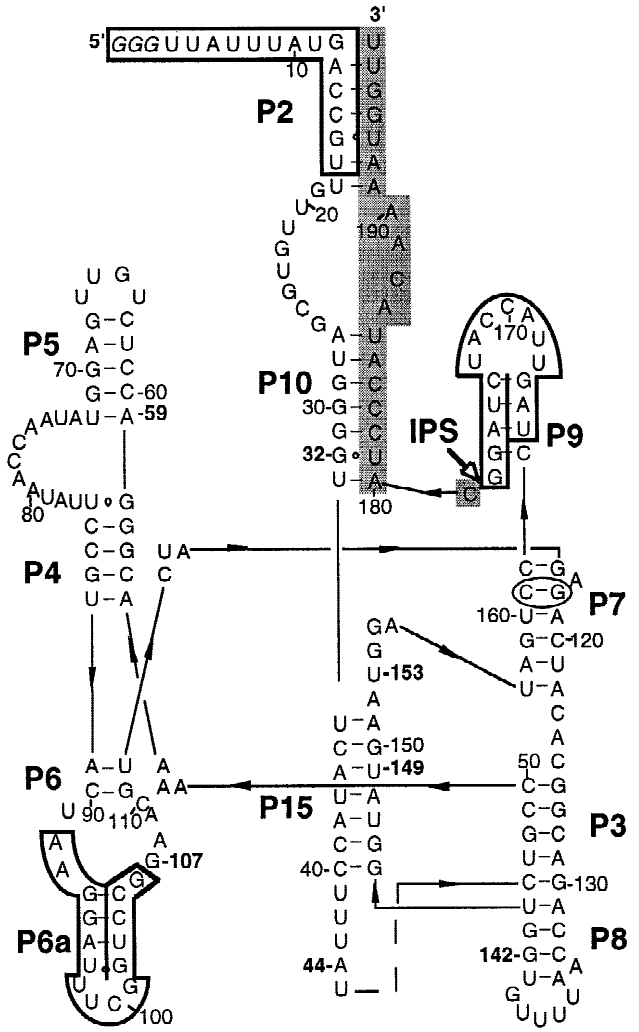

FIGURE 1. The secondary structure of the proposed reactive conformation of pre-NanGIR1 (Jabri et al., 1997). Boxed regions are those that remained constant during the selection protocol. The shaded box indicates the portion of GIR1 that is cleaved off during the selection. This region of the sequence is constant and is added back to the pool of RNA in the RT step. The G-binding site is shown in the oval.

quence comparison of the GIR1 RNAs from five species of *Naegleria* (95% sequence identity) shows that the P15 pseudoknot is highly conserved. Like NanGIR1, these other RNAs require >500 mM K^+ ions for hydrolysis at the IPS (Jabri & Cech, unpubl. data).

We set out to improve the catalytic efficiency of NanGIR1 under low-ionic-strength conditions by using in vitro selection. In this article we report the in vitro selection of GIR1 introns with greater than 300-fold improved catalytic activity. Our results show that mutagenesis of 3 nucleotides is sufficient to improve the catalytic activity 50-fold. Interestingly, these nucleotides are either within, or in proximity to, the P15 pseudoknot previously implicated as being important for hydrolytic activity.

RESULTS

Selection for enhanced activity in 100 mM K^+

To select for GIR1 RNAs with increased catalytic activity in the presence of lower concentrations of KCl, a library of sequences was prepared from two synthetic DNA oligonucleotides. These oligonucleotides were synthesized such that the resulting dsDNA molecules were randomized at the 7% level at each of the 132 nt. At this level of mutagenesis, the initial pool would have, on average, nine mutations per molecule. Sequencing of generation 0 DNA verified that each molecule had 9 ± 4 (mean ± range of 20 clones) mutations distributed throughout the partially randomized 132 nt (data not shown). Three regions of the primary sequence were kept constant during the selection (Fig. 1). The P6a stem-loop (15 nt) was kept constant for ease in generating the initial pool from two partially randomized DNA oligonucleotides. A region at the 5′ end and the 3′ end were kept constant to allow primer binding during reverse transcription (RT) and PCR. The latter constant region also allowed restoration of the processing site (base of P9 helix) after each round of selection.

The selection protocol (Fig. 2) was designed to enrich the pool with catalytically active RNA based on the ability of the RNA to cleave rapidly at the IPS in the presence of 100 mM K^+. Standard conditions for the wild-type ribozyme call for 1 M KCl (Decatur et al., 1995; Jabri et al., 1997). RNAs were preincubated at pH 5.5 to allow proper folding without hydrolysis. The reactions were initiated by the addition of buffer to increase the pH to 7.5. Active molecules, those hydrolyzing at the IPS, were separated from inactive RNA based on their faster mobility on a denaturing polyacrylamide gel. After elution of the active molecules, cDNA for another round of selection was generated by RT with the sel 2 oligonucleotide acting as the primer.

At each generation, the activity of the population was determined by measuring k_{obs} for the pool (Fig. 3A). In the initial rounds of selection, the refolding time was decreased from 30 to 5 min. After generation 2, random mutations (~1 mutation per molecule) were introduced into the RNA pool by error-prone PCR (Cadwell & Joyce, 1992). After 6 generations, the activity began to increase and in subsequent rounds surpassed the activity of pre-NanGIR1 (Fig. 3A). The selection was stopped after nine generations because the activity of the pool plateaued and the extent of the reaction decreased significantly (data not shown). RNAs from generation 8 were used in subsequent analysis since this pool cleaved to >95% completion. PCR-amplified DNAs from 62 plasmids were used as templates for run-off transcription by T7 RNA polymerase. Kinetic analyses of the individual RNA species revealed that the activities of these RNAs were widely distributed with few distinct groups (Fig. 3B). Two clones were inactive, five had

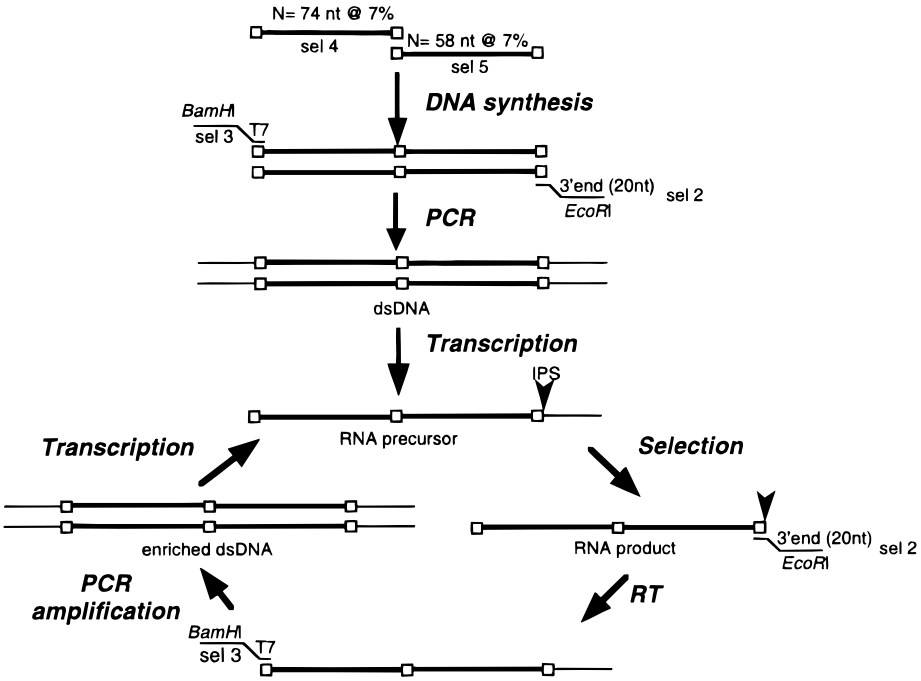

FIGURE 2. In vitro selection scheme. Details of the protocol are given in Materials and Methods. Boxes indicate constant regions required for the generation of the pool as well as RT/PCR. The selection pressure was the reaction time in 100 mM KCl. Sel 4 and sel 5 are the partially randomized (7%) DNA oligonucleotides used to generate the initial pool of RNA. Sel 2 and sel 3 are the RT/PCR primers. Sel 2 contains a 15-nt constant priming region followed by DNA coding for the 3′ end of pre-NanGIR1 (see Fig. 1) as well as an *Eco*RI restriction site. Sel 3 contains a *Bam*HI restriction site, followed by a T7 promoter region and a 15-nt constant region used for primer annealing. No detectable signal for hydrolysis product was seen on gels of generation 1–4, so markers were used to locate the expected position of this RNA.

activity within twofold of that of wild type, 11 were approximately tenfold more active, and 44 were over 100-fold more active than pre-NanGIR1.

Sequence analysis of the most active RNAs

Sequence analysis of the 56 most active clones revealed a diverse set of catalysts that, on average, contained approximately nine mutations throughout the partially randomized region of pre-NanGIR1 (data not shown). A sequence alignment of the six natural variants of GIR1 as well as the 11 most active selected clones is shown in Figure 4. The majority of the clones contain mutations in the loops of the intron. Very few mutations occur in the conserved helical elements, but this result may be because of the low level of mutagenesis used to create the initial pool. G32, a nucleotide at the base of P10, changes to an A in 34% of the clones, which converts a G·U wobble to an A-U base pair. In addition, all 4 nt at the 3′-side of the P8 helix vary, with G142 and U144 in the second and fourth base positions frequently mutated to U and A, respectively. These variations appear to disrupt the base pairing in this element, but could increase the stability of the P15 pseudoknot (e.g., U41-A144 base pair). Lastly, variations also occur at A59 and C60 at the base of the P5 helix (data not shown).

The most active clones almost always have base changes at U149 and U153 (Fig. 4). These two nucleotides are completely invariant in natural GIR1 RNAs. In 95% of the 38 most active RNAs, U149 is mutated either to a C (76%) or an A (19%). This nucleotide, located in the P15 pseudoknot, is modelled either as an A-U base pair with A36 (Fig. 5A: “reactive state”) or an unpaired U (Fig. 5B: “ground state”). U153, which is located in the unpaired region 3′ to the P15 pseudoknot, is mutated to a C in all of the active clones sequenced. The high frequency of these specific mutations in the P15 pseudoknot along with the importance of this region for activity (Jabri et al., 1997) suggested U149C and U153C could be responsible for the improved activity of the selected RNAs.

Ionic requirements of selected RNAs

The cleavage reaction of various selected RNAs was characterized with respect to their K^+ and Mg^{2+} requirements. Individual RNAs could meet the selection criteria by a variety of means. For instance, improved folding or hydrolytic activity without change in the ionic strength requirement would suffice, as would reduction in the K^+ requirement without a change in the rate under conditions of saturating K^+. The results shown in Figure 6A show that the selected RNAs display a range

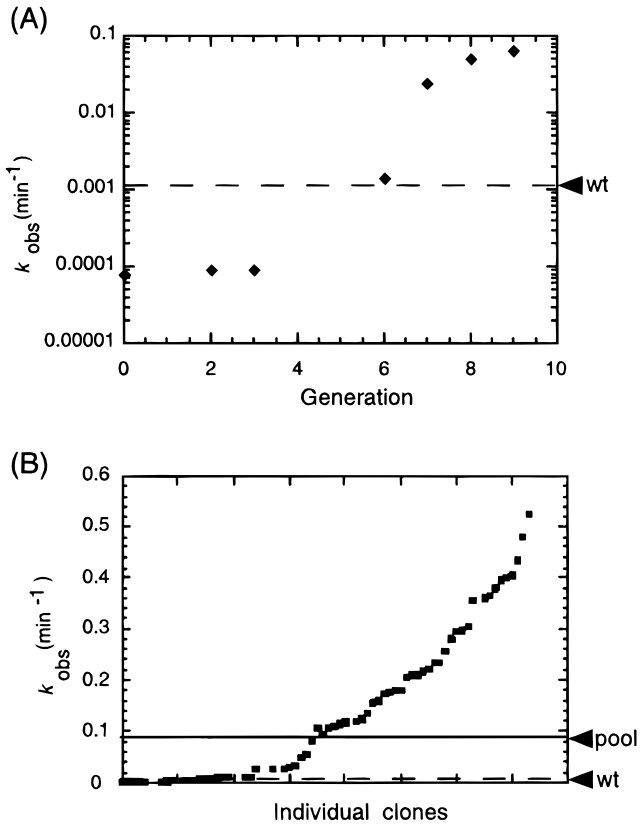

FIGURE 3. Activity of RNA pool and individual clones. **A**: The activity of each pool of RNA was assayed as follows. All RNAs were refolded for 5 min at 45 °C in 10 mM cacodylate, pH 5.5, 20 mM $MgCl_2$, and 100 mM KCl. The reaction was initiated with a pH jump to 7.5 with the addition of 4 volumes of 47.5 mM HEPES, pH 7.5, and identical $MgCl_2$ and KCl concentrations as in the refolding buffer. The fraction cleaved was then monitored as a function of time. **B**: The activity of individual generation 8 clones was determined as described above. The dashed line is pre-NanGIR1 activity under the assay conditions; the solid line indicates pool 9 activity.

of monovalent requirements. RNA 48, for instance, has a wild-type K^+ profile. RNAs 24, 32, and 65 require less K^+ (300–600 mM) for maximal activity, whereas RNA 72 requires less than 50 mM K^+. In contrast to the monovalent ion requirement, the results show that most of the RNAs require Mg^{2+} concentrations similar to that of NanGIR1 at 100 mM K^+ (Fig. 6B). A slight decrease in Mg^{2+} ion requirement is seen for RNAs 24, 48, and 72 relative to pre-NanGIR1, but, as expected, they all require Mg^{2+} ions for activity.

Thermal stability of selected RNAs

We also investigated the temperature dependence of the reactivity of these RNAs over a range of 35–65 °C. The selected RNAs had a higher $T_{(max\ activity)}$ relative to pre-NanGIR1 (Fig. 7A). These results suggest that the selection for more active ribozymes also resulted in more thermally stable GIR1 RNAs (below). Eyring analysis (Fig. 7B) of these data provided the activation parameters ($\Delta H^‡$ and $\Delta S^‡$) for the reaction of specific RNAs (Table 1). Under the selection conditions (100 mM K^+ and 20 mM Mg^{2+}), $\Delta H^‡$ and $\Delta S^‡$ for pre-NanGIR1 are large and positive. $\Delta H^‡$ decreases (favorable for reaction) by ~35 kcal/mol in the selected RNAs relative to the wild type. $\Delta S^‡$ remains positive (favorable for reaction) but not as positive, decreasing by ~100 cal/mol K. These results show that the selected RNAs achieve improved catalytic activity at lower monovalent ion concentrations through a decrease in $\Delta H^‡$ relative to pre-NanGIR1 (Table 1).

Hyperchromicity curves, which provide information on the thermal stability of the RNA tertiary structure (Puglisi & Tinoco, 1989; Banerjee et al., 1993; Laing & Draper, 1994), were completed on pre-NanGIR1 as well as a few selected RNAs. Pre-NanGIR1 melted with two transitions, one at approximately 64 °C and another at 71 °C (Fig. 8A). To distinguish which transition was due to melting of the tertiary structure, we determined the effect of monovalent ions on the melting profile of pre-NanGIR1. We have previously shown that NanGIR1 activity is sensitive to the identity of the counterion as well as its concentration (Jabri et al., 1997). Therefore, we expected that if the tertiary transition was sufficiently distinct from that of the secondary structure, we would observe a shift in this transition with increasing K^+ ions concentrations. At 325 mM K^+, the first transition had a melting temperature (T_m) of ~60 °C (Fig. 8B). The broadness of this transition is possibly due to multiple unfolding steps commonly seen with large RNAs (Puglisi & Tinoco, 1989; Laing & Draper, 1994). With increasing concentrations of K^+ ion, the T_m shifted to higher temperature (~66 °C) and the peak sharpened. This transition is unaffected by NH_4^+ or Li^+, cations that do not promote catalysis (data not shown). The second transition was unaffected by the concentration of K^+ ions in this range. The results are consistent with the first transition representing the unfolding of tertiary structure, whereas the second is the melting of secondary structure, in agreement with conclusions regarding the denaturation of self-splicing group I introns (Banerjee et al., 1993; Jaeger et al., 1993). We speculate that at low K^+ ion concentrations, the RNA is sampling multiple conformations, which results in melting with a broader transition with a lower T_m. At higher K^+ concentrations, the RNA samples fewer conformations (sharper transition) and becomes more stable to thermal denaturation (T_m (3°) = 66 °C).

Optical melts of selected RNAs 24, 48, 65, and 72 were strikingly different from those of pre-NanGIR1 (a representative example is shown in Fig. 8C). In the presence of 325 mM K^+ ions, these RNAs melted with a broad transition with a T_m between 40 and 60 °C and a sharper transition at a T_m of 67 °C. The dependence of the tertiary structure transition on monovalent ions is difficult to discern as the transition overlaps with that of the secondary structure (T_m = ~69 °C). Nevertheless,

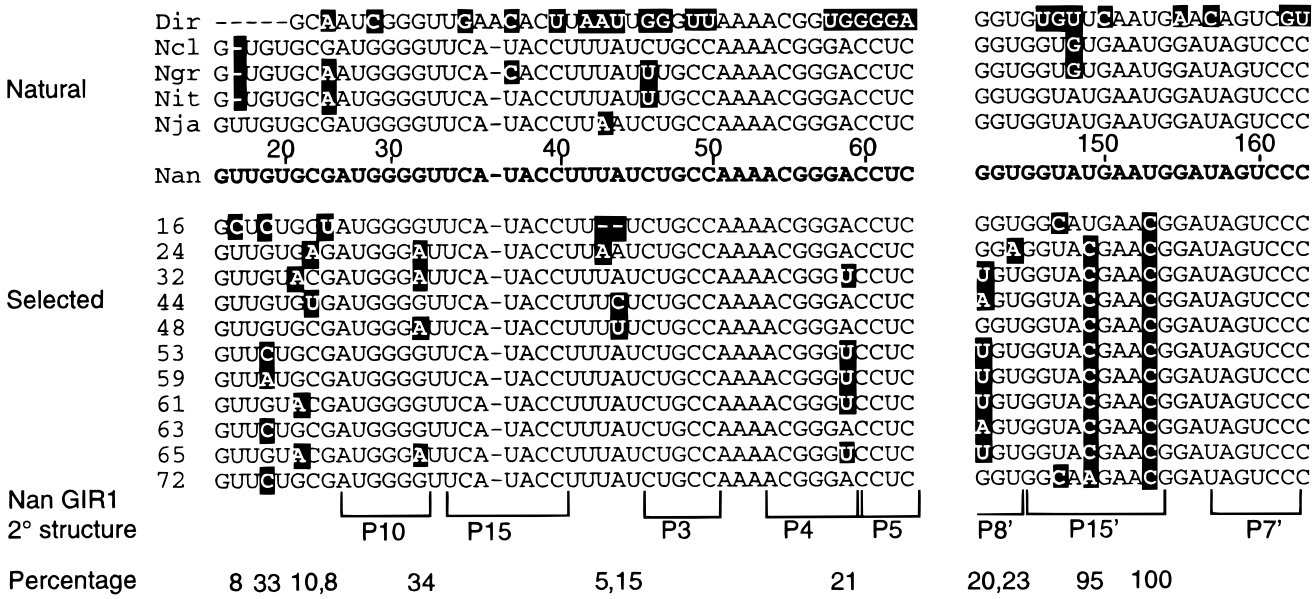

FIGURE 4. Sequence alignment of the natural and artificial variants of GIR1. Dir: *Didymium iridis*; Ncl: *Naegleria clarkii*; Ngr: *Naegleria gruberi*; Nit: *Naegleria italica*; Nja: *Naegleria jamesoni*; Nan: *Naegleria andersoni*; numbered sequences: individual selected RNAs. The secondary structure of pre-NanGIR1 is shown for reference. The reported percentage is the mutation rate in the most active selected RNA (38 total) at that position.

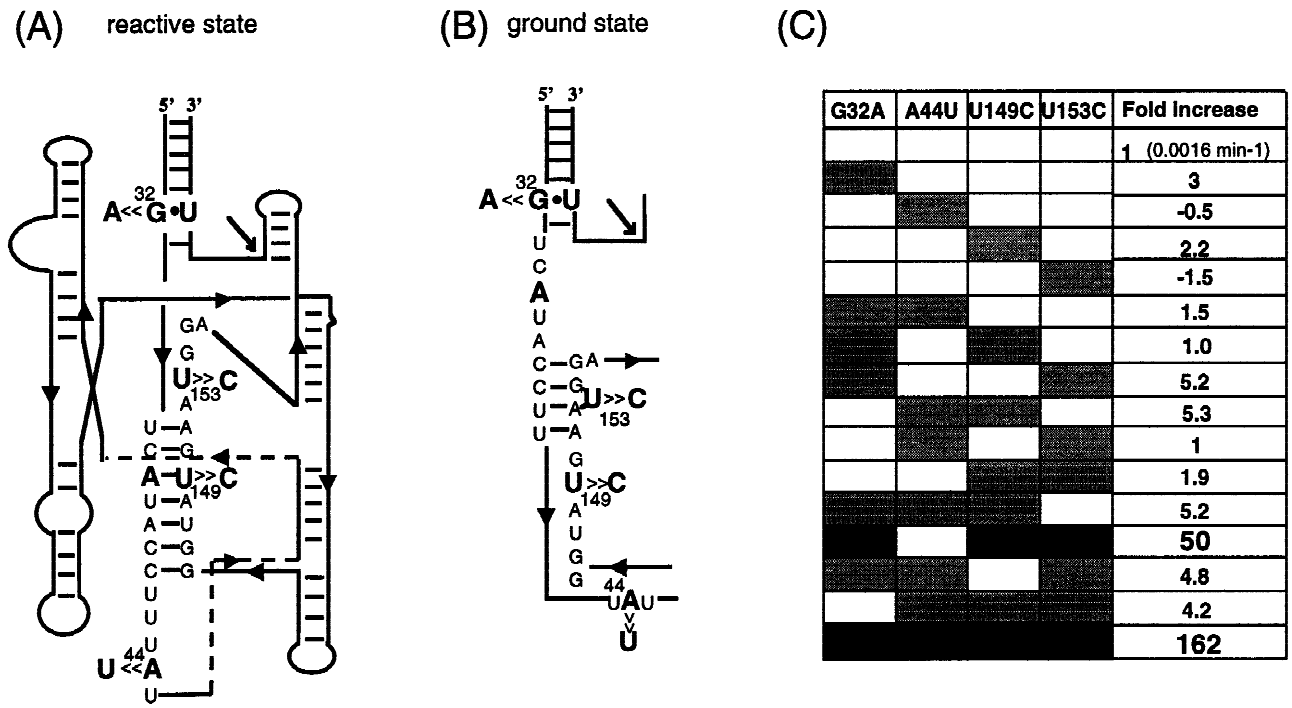

FIGURE 5. Site-directed mutagenesis was used to investigate the effect of various mutations on pre-NanGIR1 activity. All four mutations seen in RNA 48 are shown in the context of the secondary structure for pre-NanGIR1 with the P15 pseudoknot represented in **A**, a conformation based on site-directed mutagenesis studies (reactive state), and **B**, a model based on chemical modification data (ground state), which we propose to be the major conformation of the molecule under our solution conditions, but which must undergo conformational change in order to react. Only the portion of the structure that differs from **A** is shown in **B**. Note that the formation of three additional base pairs at the bottom of P15 in which A44 is paired with U149 is not supported by our chemical modification data. **C:** All permutations of the four mutations observed in RNA 48 were introduced into pre-NanGIR1 as described (see Materials and Methods). The activity of the mutants was assayed and compared to pre-NanGIR1 under the selection conditions. The gray boxes indicate the mutation(s) made. The fold increase is the activity relative to pre-NanGIR1.

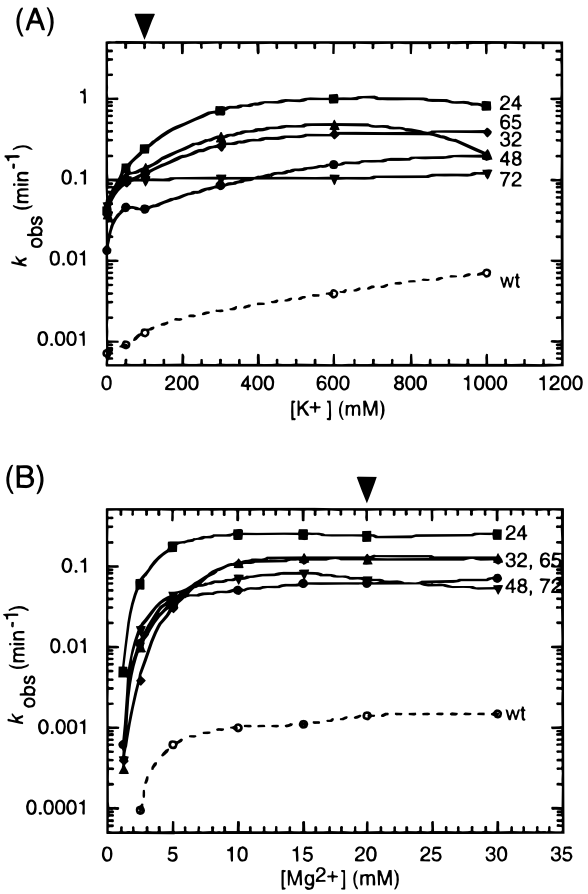

FIGURE 6. Monovalent and divalent ion requirements of the selected RNAs. **A**: K^+-ion profile of five selected RNAs in 20 mM $MgCl_2$. **B**: The Mg^{2+} profile of the same RNAs assayed in 100 mM KCl. Wild-type activity under the same conditions is plotted as the dashed line. Arrows indicate the selection conditions (100 mM K^+ and 20 mM Mg^{2+}).

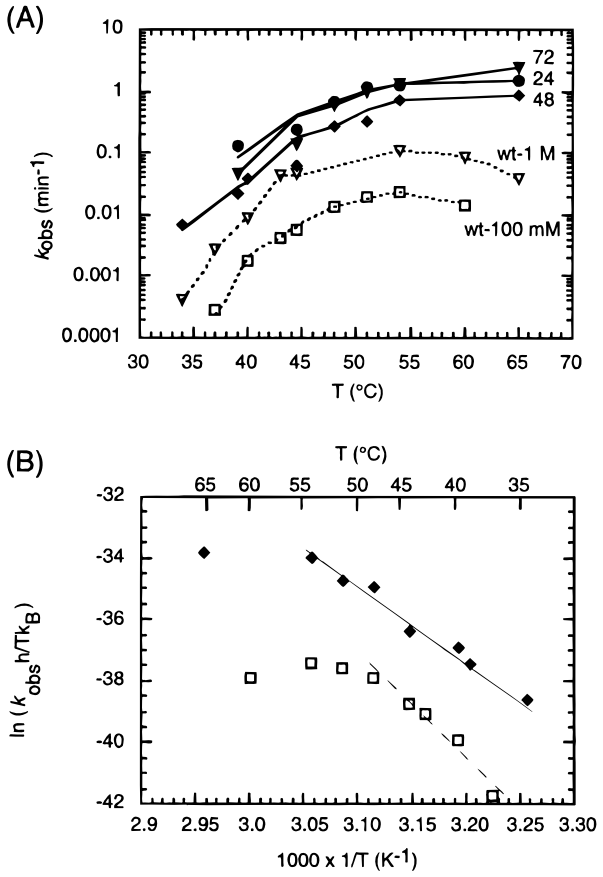

FIGURE 7. Temperature dependence of site-specific hydrolysis. **A**: k_{obs} versus temperature for three of the most active RNAs (24, 48, and 72) and pre-NanGIR1 (wt-100 mM and wt-1M, where the concentrations refer to the amount of KCl used in the reaction). The rate for pre-NanGIR1 was determined as described in Figure 3 with the exception that the refolding time was increased to 30 min, and for wt-1M, the concentration of KCl was increased to 1 M. The rates of hydrolysis for the selected RNAs, whose activities were greater than 100-fold that of pre-NanGIR1, were determined at pH 6.5. The rates were corrected for the difference in pH by using the following equation: $k_{obs}' = k_{obs} \times 10^{\Delta pH}$, where k_{obs} = measured rate constant and ΔpH = difference in pH between the pre-NanGIR1 reaction and that of the selected RNAs (~0.9). The reactions proceeded for various lengths of time at 45 °C. Each value of k_{obs} is based on the analysis of 7–12 time points. The curve fits are weighted interpolations of the data. **B**: Eyring plot of k_{obs} versus temperature for RNA 48 (diamonds) and pre-NanGIR1 (squares) in selection conditions. Data points in the linear portion of the curves (shown fit to a line) were used for the determination of $\Delta H^{\ddagger}$. h is Planck's constant, and k_B is the Boltzmann constant.

the peak does appear to shift to a T_m of ~66 °C with increasing concentrations of K^+ ions, suggesting that, like the transition for wild-type pre-NanGIR1, it is K^+ ion dependent (Fig. 8C). Overall, the T_m results indicate that even at low monovalent ion concentrations, the tertiary structures of the selected RNAs have the stability of the wild-type RNA in high K^+ concentrations.

The thermal stability of pre-NanGIR1 as well as the selected RNAs is within the range observed for other group I introns. It is more stable than the *Anabaena* intron that has a T_m (3°) of 59 °C, and is as stable as the L-21 *Sca*I *Tetrahymena* intron (T_m (3°) = 65 °C) (Banerjee et al., 1993) and the *Azoarcus* intron (T_m (3°) = 67 °C) (Tanner & Cech, 1996).

Native gel electrophoresis to assess compactness

To investigate possible effects of sequence differences on the structure of the selected RNAs, the native conformations of a representative group of the most active RNAs were investigated under the selection conditions. Nondenaturing gel electrophoresis is extensively used for studying conformational differences between wild-type and mutant RNAs (Murphy et al., 1994; Szewczak & Cech, 1997; Cao & Woodson, 1998; Pan & Woodson, 1998). Differences in migration between two molecules are generally attributed to differences in compactness. This is a particularly strong interpretation in the present case, because all molecules have the same molecular weight.

Electrophoretic mobilities of six of the most active selected precursor RNAs (197 nt) were compared to

TABLE 1. Thermal stability and activation parameters for a representative set of the most active selected RNAs.

Construct	$T_{max\ activity}$ (±2 °C)	$\Delta G^{\ddagger}_{318}$ (kcal/mol)[a]	$\Delta H^{\ddagger}$ (kcal/mol)[b]	$\Delta S^{\ddagger}_{318}$ (cal/mol K)[c]
pre-NanGIR1[d]	50	25 ± 2	70 ± 10	140 ± 12
24	≥64	22 ± 1	31 ± 1	28 ± 3
32	58	23 ± 2	33 ± 3	31 ± 5
48	60	23 ± 2	40 ± 2	53 ± 4
53	54	24 ± 2	37 ± 2	41 ± 4
65	≥64	23 ± 2	30 ± 3	22 ± 5
72	≥64	22 ± 2	41 ± 3	63 ± 5

[a] $\Delta G^{\ddagger}_{318} = -RT\ln(hk^{*}_{obs}/k_B T)$ using a standard state of the activity for water of 1; R = gas constant; T = 318 K (45 °C), h = Planck's constant, $k^{*}_{obs} = k_{obs}/60$, k_B = Boltzmann constant.

[b] $\Delta H^{\ddagger}$ as determined from fit of linear portion of Eyring plot (5–7 temperatures from 37 °C to 55 °C).

[c] $\Delta S^{\ddagger}_{318} = (\Delta H^{\ddagger} - \Delta G^{\ddagger})/T$.

[d] The large error associated with these numbers is due to the low activity of pre-NanGIR1 under these conditions, which made it difficult to measure an accurate rate.

the NanGIR1 precursor (197 nt) and the cleavage product (178 nt) (Fig. 9A). RNAs 32 and 65 had the same migration rate as pre-NanGIR1. However, RNAs 24, 48, 53, and 72 migrated faster than pre-NanGIR1, suggesting that these RNAs have more compact structures (Fig. 9B). A comparison of the sequences of these RNAs showed that many shared (in addition to U149C and U153C) two mutations, G107U and U139G. G107 is invariant whereas U139 is deleted in some natural *Naegleria* GIR1 RNAs. G107U and U139G were introduced, individually and simultaneously, into otherwise wild-type NanGIR1. The results showed that neither the single mutant nor the double mutant affects the hydrolytic activity or native gel mobility of NanGIR1 (data not shown).

Role of specific mutations in the selected RNAs

To assess directly the effect of individual bases on the improvement of catalytic activity, site-specific mutations were introduced into pre-NanGIR1. To simplify the analysis, we chose to investigate the mutations found in RNA 48. This RNA contained only four mutations, G32A, A44U, U149C, and U153C, and was 160-fold more active than pre-NanGIR1. Mutant RNAs were prepared and the cleavage rates were determined under the selection conditions (20 mM $MgCl_2$ and 100 mM KCl). As summarized in Figure 5C, only small effects were observed upon introduction of single and double mutations. Similar modest activity increases were seen with three of the four triple mutants. However, the triple mutant G32A:U149C:U153C was 50-fold more active than wild type. The combination of these three synergistic mutations is seen in 34% of the most active clones. Addition of the fourth mutation

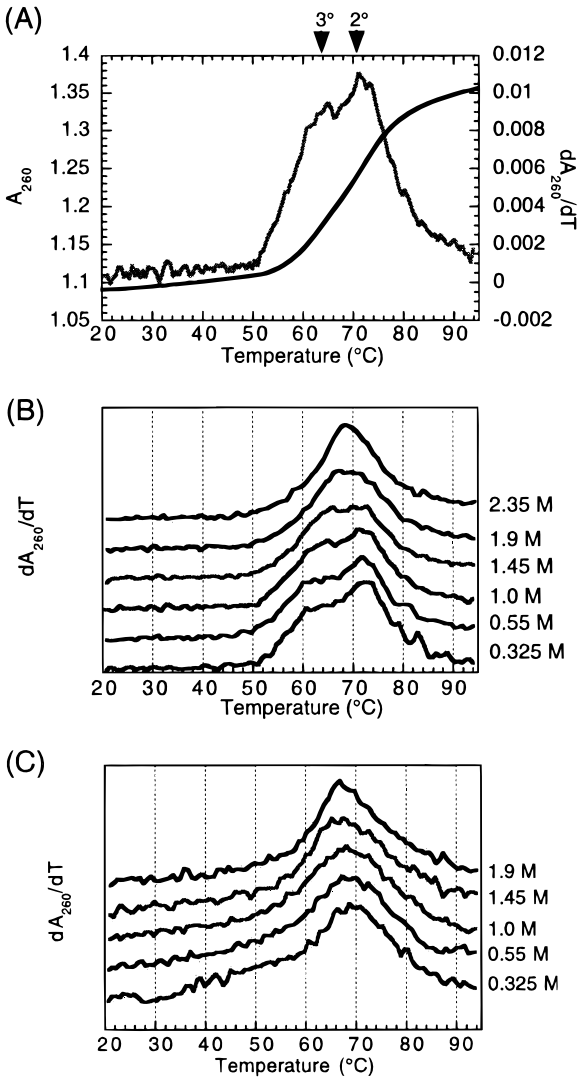

FIGURE 8. Optical melting curves of pre-NanGIR1 and RNA 48. **A**: A representative melt (black) and the derivative with respect to temperature (gray) of pre-NanGIR1 in 50 mM cacodylate, pH 5.5, 20 mM $MgCl_2$, and 1 M KCl, conditions known to support maximal activity (Jabri et al., 1997). The two transitions are attributed to the unfolding of tertiary ($T_m \sim 62$ °C) and secondary ($T_m \sim 70$ °C) structure. **B**: Denaturation of pre-NanGIR1 in increasing K^+-ion concentrations. Note that the magnitude of the 3° transition increases with increasing K^+-ion concentration, and the T_m for this transition also shifts to 68 °C. **C**: The effect of K^+ ions on RNA 48 melt. This RNA melts with one broad transition (40–60 °C) and a sharper transition with T_m = 68 °C. Similar melting curves were observed for RNAs 24, 65, and 72 with minor differences in the K^+-ion dependence of the broad transition at low T_m (data not shown).

(A44U) to this triple mutant increased activity by an additional factor of 3. When other mutations were added, such as those seen in RNA 65, activity increased up to an additional fivefold (data not shown). These results show how a few small changes throughout the RNA contribute to the improved hydrolytic activity.

The effect of such mutations on the tertiary structure of the RNA was investigated more thoroughly by analysis on native gels. The relative migration of each mu-

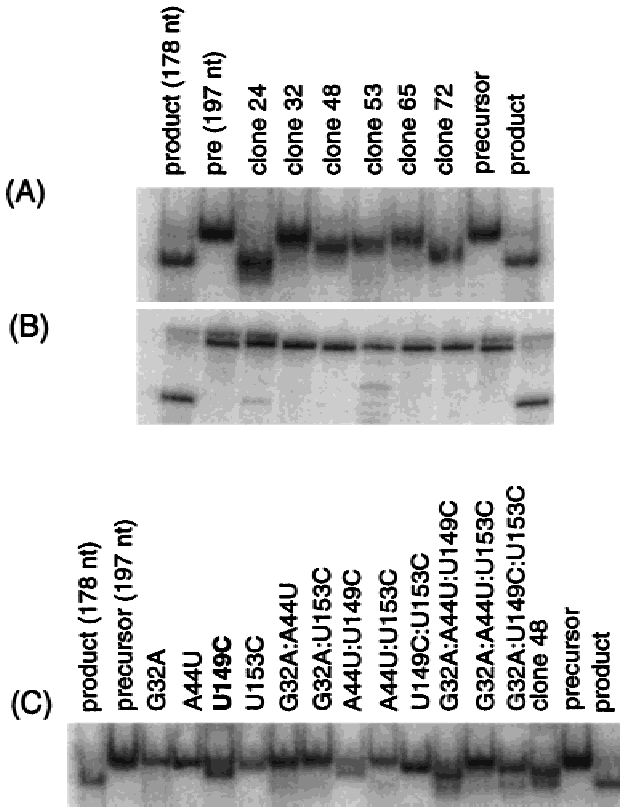

FIGURE 9. Native gel mobility of selected RNA and mutants. **A**: All RNAs were refolded and their conformational homogeneity examined by using 5% polyacrylamide gels (see Materials and Methods). **B**: Samples from **A** were examined on a 5% denaturing gel to determine relative size and composition. **C**: Gel mobility of site-directed mutants. Note that the mutation of U149C is sufficient to alter the mobility of pre-NanGIR1.

tant was compared to NanGIR1 precursor and product as well as RNA 48, which contains all four mutations. The results (Fig. 9C) show that the single mutation U149C is sufficient to increase the relative migration of more than half of the population of pre-NanGIR1. This result suggests that U149, which is located in the middle of the P15 pseudoknot (see above), makes a major contribution to the compact fold of the selected RNAs. Interestingly, addition of other mutations results in even more of the pre-NanGIR1 population migrating at the faster rate (Fig. 9C). This result is consistent with the hypothesis that pre-NanGIR1 exists as an equilibrium mixture of conformations. The mutation of certain nucleotides shifts the equilibrium towards a specific folded form.

DISCUSSION

NanGIR1 ribozyme functions optimally in the presence of 1 M K^+ ions, but is still three orders of magnitude slower than RNase P, one of the most efficient catalytic RNAs (Jabri et al., 1997). As a step towards understanding how various nucleotides in NanGIR1 affect its catalytic efficiency as well as its structure and folding, we initiated an in vitro selection experiment. The goals were (1) to generate GIR1-like molecules that were capable of undergoing hydrolysis at the IPS at a faster rate in lower concentrations of monovalent ions, and (2) to produce an artificial phylogeny for identification of key structural/functional nucleotides. We expected that more active or more stable GIR1 variants would also be useful for ongoing crystallographic studies.

We chose to randomize the native sequence of NanGIR1 at a relatively low level (7%). This procedure allows probing of the tertiary structure instead of the secondary structure because the scaffolds (i.e., helices, G-binding site) are not destroyed. Compensatory mutations are not expected because such molecules will not be represented with any appreciable frequency. We had no evidence that this low level of mutagenesis would be sufficient to improve the hydrolytic activity of GIR1. In fact, we did not know if it was even possible to improve the activity of this ribozyme. Nevertheless, the selection produced GIR1 RNAs that were greater than 300-fold more active than pre-NanGIR1 (Fig. 3B). Sequence analysis showed that many of the most active clones contained three mutations that were sufficient to increase the activity of GIR1 50-fold over pre-NanGIR1 under low salt conditions (Figs. 4 and 5C). These mutations are clustered in and around the P15 pseudoknot region of the RNA. Our results add to the growing evidence that such in vitro selection experiments can identify structurally and functionally important nucleotides in natural RNAs (Green & Szostak, 1994; Costa & Michel, 1997).

How do the selected RNAs achieve improved catalytic efficiency?

Improvements in activity can come from ground-state effects (more efficient folding or a structure closer to the transition state) and/or from transition-state effects (a structure that better stabilizes the transition state). Results of k_{obs} versus temperature and optical-melting analysis suggest that the mutations affect the ground-state structure of the selected RNAs. $T_{(max\ activity)}$ shifted to higher temperature for the most active clones (Table 1), indicating that these molecules were more thermally stable than pre-NanGIR1. In support of this conclusion, the T_m of the tertiary structure transition of the selected RNAs shifted to higher temperatures even at low concentrations of K^+ ions (Fig. 8C). Thermal melting curves of wild-type pre-NanGIR1 showed that the transition attributed to the melting of tertiary structure ($T_m \sim 66\,^{\circ}C$) shifted to a higher temperature as the concentration of K^+ ions was increased (Fig. 8B). We interpret these data to mean that at high concentrations of K^+ ions, the structure more often assumes the catalytically competent conformation. In 100 mM K^+ ion, the RNA is free to sample many conformations so

the population available to undergo site-specific hydrolysis is reduced. Unlike pre-NanGIR1, the selected RNAs achieve the catalytically competent conformation even in low concentrations of K^+ ion (Fig. 8C). Therefore, many more molecules of the selected RNAs are able to react under the selection conditions.

How do the selected RNAs achieve the proper conformation? One possibility is that these RNAs have overcome folding traps present in wild-type NanGIR1. Folding traps have been observed for the pre-rRNA and a shortened ribozyme form of the *Tetrahymena* group I intron (Downs & Cech, 1996; Zarrinkar & Williamson, 1996; Pan & Woodson, 1998; Treiber et al., 1998), and are believed to be a general feature of the folding of large RNAs. It is possible that in 100 mM K^+, wild-type NanGIR1 is kinetically trapped in structures consisting of partially native and partially non-native interactions. Refolding in 1 M K^+ removes some of the traps or facilitates the interconversion of conformational states, helping the RNA to achieve the active structure. The base changes in the selected RNAs allow them to avoid certain folding traps and therefore have improved catalytic efficiency. We are currently exploring this possibility.

An examination of the activation parameters can provide information about the transition state of the RNA. Note that the transition state may very well be that of the actual chemical cleavage step given the log-linear pH dependence of the reaction of the wild-type RNA (Jabri et al., 1997), and of several of the selected RNAs (preliminary unpubl. data). The parameters for some of the selected RNAs (Table 1) show that their reactions have a more favorable enthalpic term but a less favorable entropic term relative to pre-NanGIR1. At 45 °C, $\Delta S^{\ddagger}$ and $\Delta H^{\ddagger}$ provide approximately 32 kcal/mol and 35 kcal/mol, respectively, towards $\Delta G^{\ddagger}$ for the wild-type RNA. The large unfavorable change in $\Delta S^{\ddagger}$ upon introduction of the mutations is compensated for by a favorable change in $\Delta H^{\ddagger}$, resulting in a $\Delta\Delta G^{\ddagger}$, between wild-type GIR1 and the selected RNA, of only ~2 kcal/mol. Recall that $\Delta S^{\ddagger}$ and $\Delta H^{\ddagger}$ are not completely separable, as deformation of a reacting group to resemble more closely the transition state can serve a dual function, decreasing $\Delta H^{\ddagger}$ as well as $\Delta S^{\ddagger}$ (Jencks, 1975). Nevertheless, we can interpret the $\Delta\Delta H^{\ddagger}$ as a change in the bonding of the wild-type and selected RNAs. Therefore, it is plausible that the more favorable $\Delta H^{\ddagger}$ of the selected RNAs results from the formation of additional interactions (e.g., hydrogen bonds or stacking) in particular regions of the RNA such that the major species more accurately mimics the transition-state structure. This structural effect would decrease the energy barrier for reaching the transition state. $\Delta S^{\ddagger}$ represents the change in disorder between the ground state and this transition state. For the selected RNAs, the decrease in $\Delta S^{\ddagger}$ suggests that the increase in disorder upon reaching the transition state is smaller (less favorable for the reaction) than that of wild type. Taken together, the decreases in $\Delta H^{\ddagger}$ and $\Delta S^{\ddagger}$ suggest that in the selected RNAs, a conformational change increases the bonding between two regions of the RNA. This gives rise to additional binding energy that is used to accelerate catalysis, and is sufficiently large to overcome the unfavorable entropy of locking down a region of the RNA.

How might mutations improve hydrolytic efficiency of GIR1?

Individual mutations of G32, U149, or U153, the three most common mutations, by themselves do not significantly improve the catalytic activity relative to pre-NanGIR1. Instead, it is the introduction of all three mutations into pre-NanGIR1 that increases activity 50-fold (Fig. 5C). Additional site-directed mutagenesis results (Fig. 5C and data not shown) indicate that many of the mutations seen in other selected RNAs improve activity in the context of co-occurring mutations.

Since G32, U149, and U153 are in proximity to P15, we focused our attention on that region of the RNA. P15 is believed to be dynamic (Jabri et al., 1997). Based on chemical modification (which probes the major ground-state conformation of the RNA) and site-directed mutagenesis (which probes the transition state), we proposed that P15 consists of four base pairs in the ground state and rearranges into a seven-base-pair pseudoknot in the reactive state that precedes the transition state (Fig. 5A,B). An alternative possibility is that this region of the RNA is continuously folding and unfolding. Johansen and colleagues have proposed that, in GIR1 from *Didymium iridis*, the P15 pseudoknot also undergoes a rearrangement prior to hydrolysis (Einvik et al., 1998). In that system, the rearrangement is thought to be necessary for positioning a second cleavage site, IPS2, which is interestingly located opposite G32 (Fig. 1).

A recent molecular model for DirGIR1 (Einvik et al., 1998) shows that the 3′ side of P15 is in proximity to the P6 loop (UAAC), which in NanGIR1 would be an internal loop (GGAAC) (Fig. 1). Perhaps U149 can participate in a short-range base-pairing interaction with an A of the P6 loop, an interaction that must be disrupted for activity; the U149C mutation would then destabilize this nonproductive ground-state interaction. However, U149C would also destabilize and perhaps introduce a bend into the P15 pseudoknot (Fig. 5A), which could affect the structure of the reactive state.

U153 is an invariant nucleotide among natural GIR1 RNAs and is located in the vicinity of the P15 pseudoknot (Fig. 5A,B). The most active selected RNAs all have the U153C mutation (Fig. 4). A minimal effect on the activity (Fig. 5C) and the structure (Fig. 9C) of NanGIR1 is noted when U153 is mutated in context of pre-NanGIR1. U153 is next to G154 and G155, both of

which are implicated in metal binding in phosphorothioate substitution experiments (Jabri & Cech, unpubl. data). This nucleotide may assist in positioning other nucleotides for proper metal coordination. Furthermore, this nucleotide may contribute to shifting the backbone in the P15 pseudoknot (from Fig. 5B to 5A). Since the double mutation of U149C:U153C does not improve activity, other changes, in addition to the reregistration of P15, must take place to make the active site optimal for hydrolysis.

G32 is located at the base of P10 (Fig. 1) and forms a wobble pair with U181. This wobble pair is also conserved among all natural variants of GIR1, perhaps to create an alternative processing site IPS2 (Einvik et al., 1997). Our in vitro selection only demanded cleavage at IPS1, and it appears that the G32A mutation (seen in 34% of the most active clones; Fig. 4) enhances IPS1 cleavage. G·U pairs introduce a modest helical distortion in a duplex (Quigley & Rich, 1976; Holbrook et al., 1991; White et al., 1992). Therefore, one could speculate that the removal of even a minor distortion might result in improved positioning of the P10 helix, and possibly of G178, the guanosine at the IPS, in the G-binding site. This small change, in context of U149C:U153C, is sufficient to improve the hydrolytic activity 50-fold (Fig. 5C).

Why is the natural sequence suboptimal?

Our in vitro selection results indicate that, in the absence of protein and surrounding rRNA, we could greatly improve the catalytic efficiency of GIR1 by simply introducing three mutations in pre-NanGIR1. So we are left to wonder why nature did not make these mutations? There are numerous possible answers to this question. Johansen and colleagues suggest that the slow rate of hydrolysis for DirGIR1 is a mechanism by which the cell regulates the amount of ORF RNA and thereby the amount of homing endonuclease (Einvik et al., 1998). Based on the similarity of the *D. iridis* and *Naegleria* systems, it is likely that similar regulation would occur in all GIR1 systems. Such regulation of processing could come from simply maintaining GIR1 as an inefficient catalyst. It is also possible that in vivo, protein cofactors modulate the folding and/or activity of GIR1 (discussed by Jabri et al., 1997). Alternatively, these processes are affected by the context of GIR1 in the rRNA (for an example, see Woodson, 1992; Rocheleau & Woodson, 1995). All of the above could be life-cycle dependent and thereby limit intron mobility to certain stages in an organism's life. Ongoing in vivo and in vitro studies will surely elucidate the role of GIR1 in cellular functions.

In summary, our in vitro selection experiment (1) produced numerous catalytically competent GIR1 RNAs suitable for crystallographic analysis, (2) showed that GIR1 RNAs with improved hydrolytic activity lie close in sequence space to the pre-NanGIR1, and most importantly, (3) showed that the hydrolytic activity of GIR1 can be improved 50-fold with the mutation of only three nucleotides, G32, U149, and U153. The detailed mechanisms by which these and other nucleotides are affecting the activity are under further investigation by using biochemical and crystallographic techniques.

MATERIALS AND METHODS

Oligonucleotide synthesis

All oligonucleotides were synthesized on an Applied Biosystems DNA synthesizer, model 394. Sel 4 and sel 5 were made by using nucleoside 3′-phosphoramidite solutions that were doped with 2.33% of each of the three incorrect monomers. All oligonucleotides were gel purified prior to use.

Generation of pool

Starting material for the selection was a pool of NanGIR1 ribozyme sequences in which a 132-nt region was partially randomized. To create this pool, oligonucleotides sel 4 and sel 5, which contained the randomized regions (74 in one and 58 in the other) and a 15-nt overlapping region, were annealed and filled in with T4 DNA polymerase as follows (Fig. 2). In five separate reactions, 100 μg of sel 4 and sel 5 were mixed with annealing buffer (10 mM Tris, pH 7.5, 5 mM $MgCl_2$, and 83 mM NaCl), heated to 95 °C for 2 min, and cooled in the block to 37 °C (~30 min). The solution was then placed on ice. To this solution, $\frac{1}{5}$ volume of synthesis buffer (20 mM Tris, pH 7.5, 10 mM $MgCl_2$, 4 mM DTT, 18 mM ATP, 6 mM each GTP, CTP, and TTP) and 10 U T4 DNA polymerase were added, and the reaction incubated at 37 °C for 1 h. The enzyme was heat inactivated at 70 °C for 5 min, phenol:$CHCl_3$ extracted, ethanol precipitated, and resuspended in ddH_2O. The resulting double-stranded DNA contained 132 bases mutagenized at 7%. The random core was flanked by the 5′ and 3′ 15-nt constant regions and contained another 15-nt constant region in the middle (Fig. 1). Transcription templates were created by using PCR amplification of this cDNA with primers corresponding to the 5′ (sel 3) and 3′ (sel 2) ends of the intron sequence. Sel 3 encoded a *Bam*HI restriction endonuclease site for cloning, a promoter for T7 RNA polymerase, and sequence corresponding to the 15-nt constant region at the 5′ region of pre-NanGIR1, and sel 2 contained 15 nt complementary to the 3′ constant region, an *Ear*I site, and an *Eco*RI site. PCR was carried out for 15 cycles as previously described (Jabri et al., 1997) in ten 200 μL reactions, each containing 10 mM Tris, pH 8.3, 4 mM $MgCl_2$, 50 mM KCl, 0.2 mM each NTP, 500 pmol each primer and 5 units of *Taq* polymerase. The PCR products were pooled, ethanol precipitated, and gel purified (Qiagen protocol).

The initial RNA pool was prepared by using 40 pmol of PCR-amplified DNA by in vitro transcription of 200-μL reactions containing 40 mM Tris-HCl (pH 7.5), 5 mM $MgCl_2$, 10 mM DTT, 2 mM spermine, 2 mM each NTP, 50 μCi of α-[^{32}P] ATP, and T7 RNA polymerase. The concentration of Mg^{2+} ions was decreased to 7.5 mM in order to reduce the amount of self cleavage occurring during the transcription.

This decreased the yield, but did not affect the quality of the RNA. The reactions were incubated at 25 °C for 2–3 h, quenched with the addition of formamide stop solution (94% formamide, 0.1× TBE, 10 mM EDTA, 0.025% xylene cyanol, and 0.025% bromophenol blue), and the resulting approximately 245-nt RNA transcripts were purified on a 5% denaturing polyacrylamide gel (29:1 acrylamide:bis, 8 M urea, 1× TBE. 1× TBE is 0.1 M Tris-base, 0.083 M boric acid, and 1 mM EDTA.). Gel slices containing the labeled RNA were crushed and then soaked in TE (10 mM Tris-HCl, pH 7.5, 1 mM EDTA) at 4 °C overnight. Acrylamide was removed by filtration, and the solution was subsequently ethanol precipitated. Purified RNA was dissolved in a small volume (50 μL) of distilled, deionized water. Subsequent RNA populations were generated in 50 μL transcription reactions with 5 μCi of α-[^{32}P] ATP.

Selection and amplification strategy

The initial pool of precursor RNA was refolded prior to initiation of the cleavage reaction by using conditions developed for pre-NanGIR1 RNA: 10 mM cacodylate buffer, pH 5.5, 25 mM $MgCl_2$, and 100 mM KCl for 30 min at 45 °C . The cleavage reaction was initiated by adding 4 volumes of 50 mM HEPES, pH 7.5, also containing 25 mM $MgCl_2$ and 100 mM KCl. The reaction was incubated at 45 °C for 15 min, and quenched with ice-cold formamide stop solution. Cleaved product GIR1 was separated from precursor GIR1 by polyacrylamide gel electrophoresis and the RNA eluted from the gel slices as previously described (Jabri et al., 1997). To eliminate the DNA template, 20 units of RQ1 DNase (Promega) was added directly to the purified RNA along with 20 μL RQ1 buffer (supplied with RQ1) and the digestion was allowed to proceed for 45–60 min at 37 °C. One-tenth of a volume of 250 mM EDTA, pH 8.0, was added to the mix prior to phenol:$CHCl_3$ extraction and ethanol precipitation.

Selected RNAs were amplified following each round of selection by RT and PCR. For pool 0 RNA, the RT reaction was completed in 4 × 48-μL reactions as follows. RT primer sel 2 was annealed to the selected RNAs in 12 μL of AB buffer (50 mM Tris-base, pH 8.3, 60 mM NaCl, and 10 mM DTT) by heating to 95 °C for 1 min. An additional 12 μL AB buffer, equilibrated to 50 °C, was added prior to incubation at 50 °C. For the first amplification, the entire selected RNA was annealed to the RT primer and reverse transcribed. In subsequent rounds, only one quarter of the selected RNA pool was reverse transcribed. Reverse transcription was carried out with 1 unit of AMV reverse transcriptase (Life Sciences) in 24 μL of RT buffer (50 mM Tris, pH 8.3, 30 mM Mg-acetate, 60 mM NaCl, 10 mM DTT) in the presence of 0.5 mM each dNTP. The reactions were incubated for 20 min at 50 °C, followed by a 3-min, 95 °C incubation to heat-inactivate the enzyme. The cDNA was amplified by PCR in 100 μL reaction as previously described. The resulting double-stranded DNA was phenol:$CHCl_3$ extracted, ethanol precipitated, and transcribed for the next round of selection as described above.

The selection proceeded as follows. Generation 0 RNA was preincubated in 10 mM K-cacodylate, pH 5.5, 25 mM $MgCl_2$, and 100 mM KCl, for 30 min at 45 °C. The reaction was initiated with a pH jump to 7.5, and incubated for 15 min. For subsequent generations (1–4), the refolding protocol was modified (decreased time to 5 min). After round 2, mutageneic PCR was performed by using the method of Tsang & Joyce (1994) in order to introduce at least one additional mutation per molecule in generation 3. The selection pressure for generations 5 and 6 was increased by decreasing the reaction time to 12.5 min. A clear signal was observed for the expected product from generation 6. The selection pressure was further increased by decreasing the concentration of $MgCl_2$ (20 mM) for generation 7, followed by decreasing the reaction time to 1 min in generation 8. In addition, the volume of the DNase digestion was decreased from 200 μL to 20 μL, and that of the RT reaction to 48 μL.

Cloning and sequencing

After 8 rounds of selection and amplification, the dsDNA PCR products were digested with *Bam*HI and *Eco*RI as follows: dsDNA (50 μg) and *Bam*HI and *Eco*RI (100 U each) were combined in *Eco*RI buffer (NEB) in a total volume of 300 μL and incubated at 37 °C for 5 h. The selected dsDNAs were phenol:$CHCl_3$ extracted, ethanol precipitated, and resuspended in 20 μL TE. Resulting DNA was ligated into pUC19 plasmid and used to transform competent XL1-Blue cells by using a Bio-Rad gene pulser (1.8 kV, 400 W). Clones were screened by using restriction endonuclease digestion and verified by fluorescent cycle sequencing with dye-labeled terminators by using an ABI 377 automated sequencer from Perkin Elmer. Sequences were aligned by using the program Clustal (v. 1.5).

Activity assays

Self-cleavage reactions were carried out as described (Jabri et al., 1997) with minor modifications. Uniformly labeled RNAs were prepared as previously described with the exception that the DNA template was digested with *Eco*RI to produce an RNA of size equivalent to that used in the selection protocol. Briefly, RNA was preincubated at 45 °C for 5 min in 10 mM K-cacodylate buffer (pH 5.5), 20 mM $MgCl_2$, and 100 mM KCl. The site-specific hydrolysis reaction was initiated with a pH jump by addition of 4 volumes of 47.5 mM HEPES, pH 7.5, containing the same concentration of $MgCl_2$ and KCl as in the preincubation. Aliquots (5 μL) were removed at various intervals, and the reaction was quenched by the addition of 2 volumes of ice-cold formamide stop solution. Samples were analyzed on 5% polyacrylamide–urea gels. The gels were imaged and quantitated by using a Molecular Dynamics PhosphorImager and ImageQuant 3.0 Software. Data analysis was completed as described (Jabri et al., 1997).

Native gels

Uniformly ^{32}P-labeled GIR1 RNAs were refolded in 50 mM K-cacodylate buffer, pH 5.5, 20 mM $MgCl_2$, and 100 mM KCl at 45 °C for 5 min. Then 5× loading buffer (330 mM HEPES-acid, 170 mM Tris-base, 25% glycerol, 75 mM $MgCl_2$, 375 mM KCl) was added and the samples were immediately loaded on a 5% polyacrylamide gel (100 mM Tris-HEPES, pH 7.5, 20 mM $MgCl_2$, and 100 mM KCl). Electrophoresis proceeded at 150 V at 4 °C for approximately 8 h.

Melting curves

Optical melts were run on a Varian Cary 1E Spectrophotometer with 1.5 mL cuvettes. RNAs were prepared by run-off transcription as described above with the exception that reaction volumes were increased to 7 mL and α-[^{32}P]-ATP was omitted. After removal of the pyrophosphate precipitate, the RNA was ethanol precipitated, resuspended in 5 mL TE buffer, and purified by denaturing preparative gel electrophoresis. Samples (1 μM) were refolded at 45 °C for 30 min in 50 mM cacodylate buffer, pH 5.5, containing 20 mM $MgCl_2$ and 1 M KCl, and then diluted into 1 mL with the appropriate melt buffer (50 mM cacodylate, 20 mM $MgCl_2$, and various amounts of KCl or other monovalent salts). Absorbance data were collected at 260 and 280 nm as a function of temperature with a heating rate of 1 °C/min. Cooling curves were also taken to check for reversibility. Data points were obtained at 0.5 °C intervals. The first derivative of the absorbance-versus-temperature curve and subsequent analysis were completed by using Kaleidagraph (Abelbeck Software, v. 3.0.2).

ACKNOWLEDGMENTS

We thank Steinar Johansen for the generous gift of the Nan-290 clone from which the wild-type NanGIR1 clone was derived, and for sharing unpublished results; Volker Vogt for helpful discussion regarding the selection scheme; Cheryl Grosshans for help with making mutagenic oligos; Elaine Podell and Karen Goodrich for oligonucleotide synthesis; Anne Gooding for kinetics of natural variants; Yuming Han at the DNA sequencing facility for sequencing numerous selection clones; Robin Gutell for help with sequence analysis; Eric Westhof for providing the DirGIR1 model coordinates; and members of the Cech and Uhlenbeck labs for helpful discussion. This work was supported in part by NIH Postdoctoral Grant GM18123 to E.J. T.R.C. is an investigator of the Howard Hughes Medical Institute and an American Cancer Society Professor.

Received July 17, 1998; returned for revision August 24, 1998; revised manuscript received August 31, 1998

REFERENCES

Banerjee AR, Jaeger JA, Turner DH. 1993. Thermal unfolding of a group I ribozyme: The low-temperature transition is primary disruption of tertiary structure. *Biochemistry 32*:153–163.

Bartel DP, Szostak JW. 1993. Isolation of new ribozymes from a large pool of random sequences. *Science 261*:1411–1418.

Cadwell RC, Joyce GF. 1992. Randomization of genes by PCR mutagenesis. In: *PCR methods and applications*. Cold Spring Harbor, New York: Cold Spring Harbor Laboratory Press. pp. 28–33.

Cao Y, Woodson SA. 1998. Destabilizing effect of an rRNA stem-loop on an attenuator hairpin in the 5′ exon of the *Tetrahymena* pre-rRNA. *RNA* 4:901–914.

Costa M, Michel F. 1997. Rules for RNA recognition of GNRA tetraloops deduced by in vitro selection: Comparison with in vivo evolution. *EMBO J 16*:3289–3302.

Decatur WA, Einvik C, Johansen S, Vogt VM. 1995. Two group I ribozymes with different functions in a nuclear rDNA intron. *EMBO J 14*:4558–4568.

Downs WD, Cech TR. 1996. Kinetic pathway for the folding of the *Tetrahymena* ribozyme revealed by three UV-inducible cross-links. *RNA 2*:718–732.

Einvik C, Decatur WA, Embley TM, Vogt VM, Johansen S. 1997. *Naegleria* nucleolar introns contain two group I ribozymes with different functions in RNA splicing and processing. *RNA 3*:710–720.

Einvik C, Nielsen H, Westhof E, Michel F, Johansen S. 1998. Group I-like ribozymes with a novel core organization perform obligate sequential hydrolytic cleavage at two processing sites. *RNA 4*:530–541.

Frank DN, Pace NR. 1997. In vitro selection for altered divalent metal specificity in the RNase P RNA. *Proc Natl Acad Sci USA 94*:14355–14360.

Green R, Szostak JW. 1994. In vitro genetic analysis of the hinge region between helical elements P5-P4-P6 and P7-P3-P8 in the sun Y group I self-splicing intron. *J Mol Biol 235*:140–155.

Holbrook SR, Cheong C, Tinoco I, Kim S-H. 1991. Crystal structure of an RNA double helix incorporating a track of non-Watson–Crick base pairs. *Nature 353*:579–581.

Jabri E, Aigner S, Cech TR. 1997. Kinetic and secondary structural analysis of *Naegleria andersoni* GIR1, a group I ribozyme whose putative biological function is site-specific hydrolysis. *Biochemistry 36*:16345–16354.

Jaeger L, Westhof E, Michel F. 1993. Monitoring of the cooperative unfolding of the sunY group I intron of bacteriophage T4: The active form of the sunY ribozyme is stabilized by multiple interactions with 3′ terminal intron components. *J Mol Biol 234*:331–346.

Jencks WP. 1975. Binding energy, specificity, and enzymic catalysis: The circe effect. *Adv Enzymol 43*:219–410.

Laing LG, Draper DE. 1994. Thermodynamics of RNA folding in a conserved ribosomal RNA domain. *J Mol Biol 237*:560–576.

Lehman N, Joyce GF. 1993a. Evolution in vitro of an RNA enzyme with altered metal dependence. *Nature 361*:182–185.

Lehman N, Joyce GF. 1993b. Evolution in vitro: Analysis of a lineage of ribozymes. *Curr Biol 3*:723–734.

Murphy FL, Wang YH, Griffith JD, Cech TR. 1994. Coaxially stacked RNA helices in the catalytic center of the *Tetrahymena* ribozyme. *Science 265*:1709–1712.

Pan J, Woodson SA. 1998. Folding intermediates of a self-splicing RNA: Mispairing of the catalytic core. *J Mol Biol 280*:579–609.

Puglisi JD, Tinoco I. 1989. Absorbance melting curves of RNA. *Methods Enzymol 180*:304–325.

Quigley GJ, Rich A. 1976. Structural domains of transfer RNA molecules. *Science 194*:796–806.

Rocheleau GA, Woodson SA. 1992. Enhanced self-splicing of *Physarum polycephalum* intron 3 by a second group I intron. *RNA 1*:183–193.

Szewczak AA, Cech TR. 1997. An RNA internal loop acts as a hinge to facilitate ribozyme folding and catalysis. *RNA 3*:838–849.

Szostak JW, Ellington AD. 1993. In vitro selection of functional RNA sequences. In: Gesteland RF, Atkins JF, eds. *The RNA world*. Cold Spring Harbor, New York: Cold Spring Harbor Laboratory Press. pp. 511–533.

Tanner MA, Cech TR. 1996. Activity and thermostability of the small self-splicing group I intron in the pre-tRNA(Ile) of the purple bacterium *Azoarcus*. *RNA 2*:74–83.

Tarasow TM, Tarasow SL, Eaton BE. 1997. RNA-catalysed carbon–carbon bond formation. *Nature 389*:54–57.

Treiber DK, Rook MS, Zarrinkar PP, Williamson JR. 1998. Kinetic intermediates trapped by native interactions in RNA folding. *Science 279*:1943–1946.

Tsang J, Joyce GF. 1994. Evolutionary optimization of the catalytic properties of a DNA-cleaving ribozyme. *Biochemistry 33*:5966–5973.

White SA, Nilges M, Huang A, Brunger AT, Moore PB. 1992. NMR analysis of helix I from the 5S RNA of *Escherichia coli*. *Biochemistry 31*:1610–1621.

Woodson SA. 1992. Exon sequences distant from the splice junction are required for efficient self-splicing of the *Tetrahymena* IVS. *Nucleic Acids Res 20*:4027–4032.

Zarrinkar PP, Williamson JR. 1996. The kinetic folding pathway of the *Tetrahymena* ribozyme reveals possible similarities between RNA and protein folding. *Nat Struct Biol 3*:432–438.

Zhang B, Cech TR. 1997. Peptide bond formation by in vitro selected ribozymes. *Nature 390*:96–100.